1-2007

Antideuteron production in $\Upsilon(nS)$ decays and the nearby continuum

Roy A. Briere
Carnegie Mellon University, rbriere@andrew.cmu.edu

J. Chen

Thomas A. Ferguson
Carnegie Mellon University, ferguson@cmphys.phys.cmu.edu

G. Tatishvili
Carnegie Mellon University

Helmut Vogel
Carnegie Mellon University, helmut.vogel@cmu.edu

See next page for additional authors

Authors
Roy A. Briere, J. Chen, Thomas A. Ferguson, G. Tatishvili, Helmut Vogel, M. E. Watkins, and CLEO
Collaboration

Antideuteron production in Υ(nS) decays and the nearby continuum

D. M. Asner,[1] K. W. Edwards,[1] R. A. Briere,[2] J. Chen,[2] T. Ferguson,[2] G. Tatishvili,[2] H. Vogel,[2] M. E. Watkins,[2]
J. L. Rosner,[3] N. E. Adam,[4] J. P. Alexander,[4] K. Berkelman,[4] D. G. Cassel,[4] J. E. Duboscq,[4] K. M. Ecklund,[4] R. Ehrlich,[4]
L. Fields,[4] R. S. Galik,[4] L. Gibbons,[4] R. Gray,[4] S. W. Gray,[4] D. L. Hartill,[4] B. K. Heltsley,[4] D. Hertz,[4] C. D. Jones,[4]
J. Kandaswamy,[4] D. L. Kreinick,[4] V. E. Kuznetsov,[4] H. Mahlke-Krüger,[4] T. O. Meyer,[4] P. U. E. Onyisi,[4] J. R. Patterson,[4]
D. Peterson,[4] E. A. Phillips,[4] J. Pivarski,[4] D. Riley,[4] A. Ryd,[4] A. J. Sadoff,[4] H. Schwarthoff,[4] X. Shi,[4] S. Stroiney,[4]
W. M. Sun,[4] T. Wilksen,[4] M. Weinberger,[4] S. B. Athar,[5] P. Avery,[5] L. Breva-Newell,[5] R. Patel,[5] V. Potlia,[5] H. Stoeck,[5]
J. Yelton,[5] P. Rubin,[6] C. Cawlfield,[7] B. I. Eisenstein,[7] I. Karliner,[7] D. Kim,[7] N. Lowrey,[7] P. Naik,[7] C. Sedlack,[7] M. Selen,[7]
E. J. White,[7] J. Wiss,[7] M. R. Shepherd,[8] D. Besson,[9] T. K. Pedlar,[10] D. Cronin-Hennessy,[11] K. Y. Gao,[11] D. T. Gong,[11]
J. Hietala,[11] Y. Kubota,[11] T. Klein,[11] B. W. Lang,[11] R. Poling,[11] A. W. Scott,[11] A. Smith,[11] S. Dobbs,[12] Z. Metreveli,[12]
K. K. Seth,[12] A. Tomaradze,[12] P. Zweber,[12] J. Ernst,[13] H. Severini,[14] S. A. Dytman,[15] W. Love,[15] V. Savinov,[15]
O. Aquines,[16] Z. Li,[16] A. Lopez,[16] S. Mehrabyan,[16] H. Mendez,[16] J. Ramirez,[16] G. S. Huang,[17] D. H. Miller,[17]
V. Pavlunin,[17] B. Sanghi,[17] I. P. J. Shipsey,[17] B. Xin,[17] G. S. Adams,[18] M. Anderson,[18] J. P. Cummings,[18] I. Danko,[18]
J. Napolitano,[18] Q. He,[19] J. Insler,[19] H. Muramatsu,[19] C. S. Park,[19] E. H. Thorndike,[19] T. E. Coan,[20] Y. S. Gao,[20] F. Liu,[20]
M. Artuso,[21] S. Blusk,[21] J. Butt,[21] J. Li,[21] N. Menaa,[21] R. Mountain,[21] S. Nisar,[21] K. Randrianarivony,[21] R. Redjimi,[21]
R. Sia,[21] T. Skwarnicki,[21] S. Stone,[21] J. C. Wang,[21] K. Zhang,[21] S. E. Csorna,[22] G. Bonvicini,[23] D. Cinabro,[23]
M. Dubrovin,[23] and A. Lincoln[23]

(CLEO Collaboration)

[1]*Carleton University, Ottawa, Ontario, Canada K1S 5B6*
[2]*Carnegie Mellon University, Pittsburgh, Pennsylvania 15213, USA*
[3]*Enrico Fermi Institute, University of Chicago, Chicago, Illinois 60637, USA*
[4]*Cornell University, Ithaca, New York 14853, USA*
[5]*University of Florida, Gainesville, Florida 32611, USA*
[6]*George Mason University, Fairfax, Virginia 22030, USA*
[7]*University of Illinois, Urbana-Champaign, Illinois 61801, USA*
[8]*Indiana University, Bloomington, Indiana 47405, USA*
[9]*University of Kansas, Lawrence, Kansas 66045, USA*
[10]*Luther College, Decorah, Iowa 52101, USA*
[11]*University of Minnesota, Minneapolis, Minnesota 55455, USA*
[12]*Northwestern University, Evanston, Illinois 60208, USA*
[13]*State University of New York at Albany, Albany, New York 12222, USA*
[14]*University of Oklahoma, Norman, Oklahoma 73019, USA*
[15]*University of Pittsburgh, Pittsburgh, Pennsylvania 15260, USA*
[16]*University of Puerto Rico, Mayaguez, Puerto Rico 00681*
[17]*Purdue University, West Lafayette, Indiana 47907, USA*
[18]*Rensselaer Polytechnic Institute, Troy, New York 12180, USA*
[19]*University of Rochester, Rochester, New York 14627, USA*
[20]*Southern Methodist University, Dallas, Texas 75275, USA*
[21]*Syracuse University, Syracuse, New York 13244, USA*
[22]*Vanderbilt University, Nashville, Tennessee 37235, USA*
[23]*Wayne State University, Detroit, Michigan 48202, USA*

Using CLEO data, we study the production of the antideuteron, $\bar{d}$, in Υ(nS) resonance decays and the nearby continuum. The branching ratios obtained are $\mathcal{B}^{\text{dir}}(\Upsilon(1S) \rightarrow \bar{d}X) = (3.36 \pm 0.23 \pm 0.25) \times 10^{-5}$, $\mathcal{B}(\Upsilon(1S) \rightarrow \bar{d}X) = (2.86 \pm 0.19 \pm 0.21) \times 10^{-5}$, and $\mathcal{B}(\Upsilon(2S) \rightarrow \bar{d}X) = (3.37 \pm 0.50 \pm 0.25) \times 10^{-5}$, where the ''dir'' superscript indicates that decays produced via reannihilation of the $b\bar{b}$ pair to a γ^* are removed from both the signal and the normalizing number of Υ($1S$) decays in order to isolate direct decays of the Υ($1S$) to ggg, $gg\gamma$. Upper limits at 90% C.L. are given for $\mathcal{B}(\Upsilon(4S) \rightarrow \bar{d}X) < 1.3 \times 10^{-5}$, and continuum production $\sigma(e^+e^- \rightarrow \bar{d}X) < 0.031$ pb. The Υ($2S$) data is also used to extract a limit on $\chi_{bJ} \rightarrow \bar{d}X$. The results indicate enhanced deuteron production in ggg, $gg\gamma$ hadronization compared to $\gamma^* \rightarrow q\bar{q}$. Baryon number compensation is also investigated with the large Υ($1S$) $\rightarrow \bar{d}X$ sample.

I. INTRODUCTION

Antideuteron production has been observed in e^+e^- collisions at both the $\Upsilon(1S)$ [1] and Z [2] resonances as well as in a variety of other interactions [3]. The study of antideuterons rather than deuterons avoids large backgrounds from interactions with beam gas and detector material in colliders and nuclear breakup in fixed-target and heavy ion collisions. Since the various hadronization processes we wish to explore are expected to be charge symmetric, there is no loss of information incurred by studying only the experimentally cleaner antideuterons.

Theoretical descriptions of antideuteron formation are generally based on a coalescence model, according to which an antineutron and antiproton nearby to each other in phase space bind together [4]. Simple calculations may be based on empirical antibaryon production rates, but subtleties arise. Nearby in phase space largely means nearby in vector momentum since the hadronization occurs in a compact region. But the finite size of this region and the presence of short-lived intermediate resonances, such as the $\bar{\Delta}$ quartet, lead to questions concerning the necessary degree of coherence, which can only be addressed with further assumptions. The combined $\Upsilon(1S)$, $\Upsilon(2S)$ result from ARGUS [1] as well as an upper limit from OPAL at the Z [5] were accommodated by Gustafson and Hakkinen [6] on the basis of a string model calculation used to supply details of the fragmentation process. ALEPH [2] also compared their recent result to this model but limited precision and momentum range proscribe any definitive conclusions. A more accurate experimental result is desirable to further refine models.

Practical limitations of particle identification restrict the momentum range over which antideuterons may be studied. However, the lower mass of the $\Upsilon(1S)$ means that a larger fraction of the momentum spectrum is accessible compared to experiments at the Z pole. Also, baryon production in $\Upsilon(1S)$ decays is known to be enhanced relative to continuum hadronization [7]. The Z pole provides a generous rate enhancement but the hadronization proceeds via an initial $q\bar{q}$ pair just as the e^+e^- continuum, whereas the $\Upsilon(1S)$ decays primarily via three gluons which may be contrasted with nearby continuum $q\bar{q}$ data. Gluerich $\Upsilon(1S)$ decays might also produce exotic multiquark states, beyond $q\bar{q}$ and qqq [8]. As with antideuterons, these may form in a similar coalescence process of intermediate hadrons or from the primary ggg, $gg\gamma$ hadronization [9]. It is also interesting to search for evidence of antideuteron production inconsistent with coalescence. The frequency with which baryon number is compensated via two baryons compared to a deuteron accompanying the antideuteron may prove useful in this regard.

Our key result will be a much-improved determination of the rate of antideuteron production from $\Upsilon(1S) \rightarrow ggg$, $gg\gamma$ hadronization. The momentum dependence of production may help discriminate production models and is

also used to estimate production outside our experimentally accessible momentum range. Given the larger data samples, we do not need to combine $\Upsilon(1S)$ and $\Upsilon(2S)$ production as done [1] previously, but instead use the $\Upsilon(2S)$ data to limit $\chi_{bJ}(1P)$ production of antideuterons. In addition, we obtain a first limit on antideuterons from the $\Upsilon(4S)$ and an improved limit on continuum production.

II. DATA AND SELECTION CRITERIA

We use data collected with the CLEO detector at the Cornell Electron Storage Ring, at or near the energies of the $\Upsilon(nS)$ resonances, where $n = 1, 2, 4$. The analyzed event samples correspond to integrated luminosities of 1.2 fb^{-1} on the $\Upsilon(1S)$, 0.53 fb^{-1} on the $\Upsilon(2S)$, 0.48 fb^{-1} on the $\Upsilon(4S)$, and 0.67 fb^{-1} of continuum data from just below the $\Upsilon(4S)$. The resonance samples contain a total of 21.95×10^6 $\Upsilon(1S)$, 3.66×10^6 $\Upsilon(2S)$, and 0.45×10^6 $\Upsilon(4S)$ decays.

Smaller effective cross sections on the $\Upsilon(2S)$ and $\Upsilon(3S)$ and complications from feed-down decrease yields and complicate interpretation of these data. Thus, we will emphasize the $\Upsilon(1S)$ sample. The $\Upsilon(2S)$ sample is used to limit antideuteron production from $\chi_{bJ}(1P)$ decays by assuming that the ggg, $gg\gamma$ production from the $\Upsilon(1S)$ and $\Upsilon(2S)$ are identical. We choose not to analyze an available $\Upsilon(3S)$ sample since the statistical error on a branching ratio would be quite large. It would also not be possible to separate the contributions from $\Upsilon(1S)$, $\Upsilon(2S)$, $\chi_{bJ}(1P)$, and $\chi_{bJ}(2P)$ feed-down from the direct $\Upsilon(3S)$ decays in a meaningful way.

The four innermost portions of the CLEO detector are immersed in a 1.5 T solenoidal field. Charged-particle tracking is provided by a four-layer double-sided silicon microstrip detector [10] and a 47-layer small-cell drift chamber with one outer cathode layer [11]. The drift chamber also provides particle identification via specific ionization (dE/dx) measurements. Surrounding the drift chamber is a LiF-TEA ring-imaging Cherenkov (RICH) detector [12], followed by a CsI(Tl) calorimeter [13]. Most critical in the current analysis are the drift chamber, which covers $|\cos\theta| < 0.93$, and the RICH detector, which covers $|\cos\theta| < 0.80$, where θ is the polar angle with respect to the e^+e^- beams.

Our antideuteron track selection proceeds as follows. First, a candidate charged track must be consistent with originating from the interaction point. The impact parameter with respect to the nominal collision point along the beam direction, Δz, must satisfy $|\Delta z| < 0.05$ m; this distribution is dominated by the physical beam bunch length. The impact parameter in the $r - \phi$ plane perpendicular to the beam, Δr, is required to satisfy $|\Delta r| < 0.005$ m. Since the transverse beam size is much smaller, the difference here is taken with respect to a time-averaged collision point to account for accelerator lattice changes and other effects. The collision point can be stable over many days for a fixed

lattice. The track must be well measured, based on the reduced χ^2 of the track fit and the fraction of traversed drift-chamber layers with good hits. Because of difficulties in reconstructing low-momentum tracks (especially considering the large energy loss of the softest antideuterons in material before the drift chamber) and the shrinking dE/dx separation between antideuterons and other species at high momentum, we only consider tracks with momenta between 0.45 GeV/c and 1.45 GeV/c. We will later estimate the amount of signal outside this momentum interval.

The identification of a quality track as an antideuteron relies on the ionization energy loss measurement in the drift chamber (dE/dx). To ensure a high-quality dE/dx measurement, we only use tracks with at least 10 charge samplings remaining after truncation of the highest 20% and lowest 5% of the charge samples for each track. This particular truncation was chosen to optimize the resolution for a sample of electrons and positrons distributed uniformly in solid angle. Further, the track angle with respect to the beam line, θ, must satisfy $|\cos\theta| > 0.2$ in order to avoid large gas-gain saturation effects present at normal incidence with respect to the chamber wires. This limit was chosen by examining the behavior of the large inclusive deuteron sample and observing where the success of the corrections applied to compensate for this saturation begin to degrade.

The dE/dx measurement is converted to a normalized deviation

$$\chi_d \equiv \frac{(dE/dx)_{\text{measured}} - (dE/dx)_{\text{expected},d}}{\sigma_{dE/dx}} \qquad (1)$$

with respect to the ionization expected for a real (anti)-deuteron. The dE/dx expected mean and resolution (σ) include dependencies on velocity ($\beta\gamma = p/m$), $\cos\theta$, and the number of hits used to obtain the measured dE/dx. We accept a track as a deuteron candidate if $-2 < \chi_d < +3$; the asymmetric cut is chosen to reduce background from the large number of protons, which appear at lower values of dE/dx. The lowest momentum antideuterons considered here produce a raw charge deposition on the drift-chamber wires about 10 times larger than a minimum-ionizing particle. The electronic readout has sufficient dynamic range to fully accommodate this.

To suppress π and p background, we impose requirements on the number of detected Cherenkov photons in the RICH detector. Proton suppression is important since they are nearest to deuterons in ionization, while suppression of pions is added since they are so numerous; kaon suppression is not employed. For a given particle hypothesis, only photons within 3 standard deviations of the expected ring location are counted; we require fewer than five photons for the π hypothesis and fewer than three photons for the p hypothesis. For the entire momentum range, pions are well above Cherenkov threshold and give more than 10 detected photons on average, while protons cross threshold near

$p = 0.9$ GeV/c with the mean number of photons increasing with increasing momentum.

III. YIELD EXTRACTION AND BACKGROUNDS

Our signal is typified by a well-reconstructed track coming from the interaction point, with dE/dx consistent with an antideuteron. We choose to use the distribution of the normalized deviation, χ_d, to determine our raw signal yield. We do this in five 200 MeV/c momentum bins spanning 0.45–1.45 GeV/c.

The backgrounds to our antideuteron signal are from three main sources. The first is particle misidentification. For most of the momentum range considered, dE/dx separation is good; however, since antideuterons are very rare compared to the other hadrons, even a small resolution or mismeasurement tail may be troublesome. Second, spurious hadrons are produced via interactions of beam particles or genuine decay products with residual gas in the beampipe or the beampipe and inner detector material. In practice, this is a much larger issue for deuterons than antideuterons since the gas and material are matter and not antimatter. This is the primary reason we focus on antideuterons in this study. Finally, for resonance decays, there is a possible nonresonant contribution from the continuum events underlying the Υ resonance peaks.

Our raw yield and the particle misidentification background are determined as follows. We count the total number of entries between $-2 < \chi_d < +3$, denoting this as N. The efficiency of this cut will be discussed below, in Sec. IV B. To estimate the background from misidentification, we fit the χ_d distribution to a Gaussian signal peak plus an exponential background shape, as shown in Fig. 1. The mean and width of the Gaussian are fixed from fits to the larger deuteron sample in the data. We then define a triangular background shape as shown in Fig. 1. The apex lies on the background curve at the χ_d value corresponding to the minimum of the total fit function, between the rapidly falling background and the signal peak. The triangle is drawn to decrease to zero height at $\chi_d = +3$. We denote the area of this triangle between $-2 < \chi_d < +3$ as A. We then take the central value of the raw yield as $N - A/2$ with an error of $\pm A/4$. The rapidly falling fit would argue for a lower background, while a small accumulation of events at $\chi_d > +3$ balances this. In fact, we know little about the background shape other than naively expecting a falling shape. Our method spans the range from 0 to A for the background size within $\pm 2\sigma$, where $\sigma = A/4$.

For beam particles or decay products interacting with residual gas or beampipe and detector material, the tracks do not peak in both $r - \phi$ and z impact parameters as the signal does. We therefore estimate the underlying background from these sources by looking at the impact-parameter sidebands. These backgrounds are small and assumed to be flat for purposes of the modest extrapolation underneath the peaks.
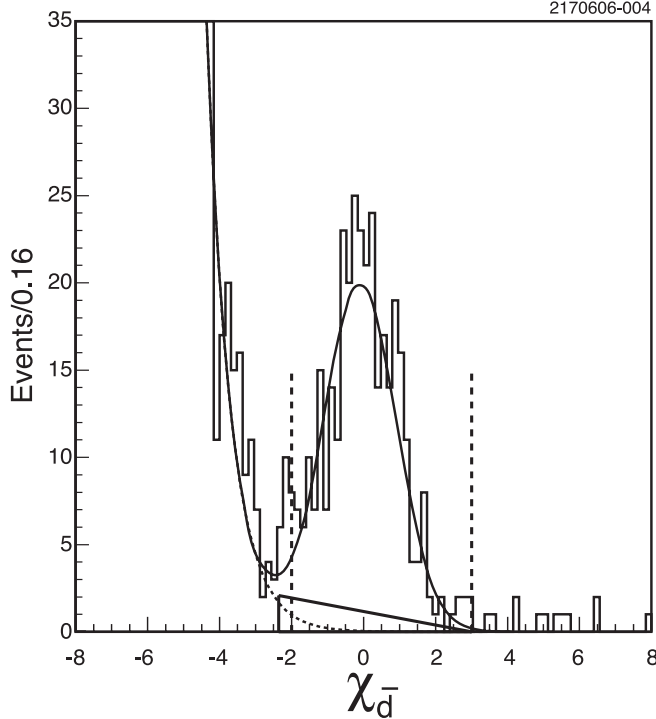
FIG. 1. The χ_d distribution in the momentum range 0.45–1.45 GeV/c fit to a Gaussian antideuteron signal and a falling background function. The background estimation employs the area of the triangular region between the dashed cuts, as detailed in the text.

The nonresonant contribution is estimated through analysis of our off-resonance data sample. Since this contribution is found to be small, we use data taken below the $\Upsilon(4S)$ resonance to subtract it for all Υ resonances. The off-resonance data is scaled by a factor accounting for the ratio of luminosities and the $1/s$ dependence of the cross section with respect to the resonance sample. We will also consider the process $\Upsilon(nS) \rightarrow \gamma^* \rightarrow q\bar{q}$ as background, because the physics is the same as the continuum $e^+ e^- \rightarrow q\bar{q}$ process, and we are interested primarily in the ggg and $gg\gamma$ decays of the Υ. Thus, when subtracting continuum yields, we adjust the scale factor to account for the additional continuumlike events produced via reannihilation into a γ^*. Similarly, the most useful branching ratio will be normalized not to the total number of decays, $N(\Upsilon(nS))$, but instead to

$$N_{\rm dir} = N(\Upsilon(nS))(1 - (3 + R_{\rm had})\mathcal{B}_{\mu\mu}), \qquad (2)$$

counting only the decays proceeding via ggg, $gg\gamma$ hadronization by excluding dilepton decays, which proceed via a γ^* as well. Here, $\mathcal{B}_{\mu\mu} = \mathcal{B}(\Upsilon(nS) \rightarrow \mu^+ \mu^-)$ and $R_{\rm had} = \sigma(e^+ e^- \rightarrow {\rm hadrons})/\sigma(e^+ e^- \rightarrow \mu^+ \mu^-)$. The factors of 3 and $R_{\rm had}$ scale the value of $\mathcal{B}_{\mu\mu}$ to account for the sum of $e^+ e^-$, $\mu^+ \mu^-$, $\tau^+ \tau^-$, and the sum of allowed $q\bar{q}$ pairs, respectively. We use $R_{\rm had} = 3.56 \pm 0.01 \pm 0.07$ [14] and $\mathcal{B}_{\mu\mu} = (2.49 \pm 0.02 \pm 0.07)\%$ [15].

TABLE I. Antideuteron yields and backgrounds for $\Upsilon(1S)$ data in momentum bins.

Momentum (GeV/c)	On $\Upsilon(1S)$	Continuum	Δr sideband	Δz sideband
0.45–0.65	60.4 ± 7.9	2.0 ± 1.4	9.0 ± 3.0	6.0 ± 2.5
0.65–0.85	77.9 ± 9.2	1.0 ± 1.0	2.0 ± 1.4	4.0 ± 2.0
0.85–1.05	71.0 ± 8.9	$0.0^{+1.2}_{-0.0}$	1.0 ± 1.0	$0.0^{+1.2}_{-0.0}$
1.05–1.25	58.1 ± 7.8	$0.0^{+1.2}_{-0.0}$	$0.0^{+1.2}_{-0.0}$	$0.0^{+1.2}_{-0.0}$
1.25–1.45	46.4 ± 7.2	3.0 ± 1.7	$0.0^{+1.2}_{-0.0}$	2.0 ± 1.4

We refer to the resulting branching ratio as the "direct" one. This branching ratio is equivalent to

$$\mathcal{B}^{\rm dir}(\Upsilon(1S) \rightarrow \bar{d}X) = \frac{\mathcal{B}(\Upsilon(1S) \rightarrow ggg, gg\gamma \rightarrow \bar{d}X)}{\mathcal{B}(\Upsilon(1S) \rightarrow ggg, gg\gamma \rightarrow X)}. \qquad (3)$$

This will be our central result concerning ggg, $gg\gamma$ hadronization. For completeness, we also present a conventional branching ratio without the modifications described in the preceding paragraph. Since we will find that continuum production of antideuterons is small, while non-ggg, $gg\gamma$ decays of the $\Upsilon(1S)$ are significant, the direct branching ratio will be larger than the conventional inclusive one.

Results of the above yield and background determinations are summarized in Table I.

IV. DETECTION EFFICIENCY

A. Tracking and rich efficiency

We use Monte Carlo (MC) event samples to study the antideuteron efficiency of our tracking and RICH criteria. We cannot use antideuterons in our simulations since this particle is not included in GEANT, which is the basis of CLEO Monte Carlo software. However, we do not expect significant differences between deuteron and antideuteron behavior since both the RICH detector and the tracking are largely charge independent, as are our selection criteria. Nuclear interactions do distinguish d and $\bar{d}$, but given our large final errors, we may safely neglect this effect as well. In particular, annihilations in the beampipe or silicon vertex detector are estimated to be negligible given our statistics. We also note that our Υ decay hadronization models produce very few deuterons; this leads us to choose the following techniques.

Our first Monte Carlo sample consists of events with one deuteron and no other detector activity. The second consists of overlaying the preceding type of "single-track" events on top of a real $\Upsilon(1S)$ decay from data. The former likely overestimates the efficiency due to the quiet detector environment, while the latter likely underestimates it due to excess activity (since nothing is removed from the full decay when the signal track is added in). We obtain tracking efficiencies of about 70%, with a 10% relative difference between the two methods. Our definition of efficiency

is relative to the number of tracks entering the active tracking volume; two-thirds of the loss is due to the exclusion of tracks with small polar angles mentioned earlier.

We average the efficiencies of our two Monte Carlo samples, taking one-quarter of the difference between them as a systematic uncertainty. The resulting efficiency is fairly flat, except in the lowest momentum bin of 0.45–0.65 GeV/c, where it decreases by about 10% of itself. By reweighting Monte Carlo events according to the momentum distribution of the data across this bin, we find that we are not very sensitive to the detailed spectrum, but we do add an additional systematic error for this effect.

Finally, our signal is consistent with being flat vs $\cos\theta$ in the accepted range $0.20 < |\cos\theta| < 0.93$; we assume it is flat when evaluating the effect of our fiducial cut on the track-finding efficiency.

B. dE/dx efficiency

The CLEO Monte Carlo simulation of dE/dx measurements is done at the track level and is based on the calibrated expected means and resolutions. However, (anti)deuterons have not been searched for in any other CLEO analysis to date. Since the calibration is quite challenging for the very high ionization of the lower momentum antideuterons, the dE/dx calibration was redone for the data samples used here. These new calibrations offer less bias versus parameters such as angle and momentum than the standard versions. But, as a result, the CLEO dE/dx simulation designed for the standard calibration is not well suited for our analysis. Instead, we use deuterons from real data, produced by beam-gas interactions, to estimate the dE/dx efficiency. Our impact parameter cuts ensure that these tracks are geometrically similar to signal tracks.

Figure 2 shows the deuteron χ_d distributions for all five momentum bins; these are mostly deuterons from beam-gas interactions or nuclear interactions in the detector. We define the dE/dx signal efficiency as $\epsilon_{dE/dx} = N_{\rm sig}/N_d$, where $N_{\rm sig}$ is the yield in the interval $-2 < \chi_d < +3$ and N_d is our estimate of the total number of deuterons for all χ_d. We estimate $N_d = (N_{\rm tot} - N_{\rm tail}/2) \pm N_{\rm tail}/4$. Here $N_{\rm tot}$ is the yield in the interval $-5 < \chi_d < +5$ for the lowest two bins, in $-4 < \chi_d < +4$ for the next two, and in $-3 < \chi_d < +4$ for the highest momentum bin. $N_{\rm tail}$ is designed to include a possible tail from the large background at low χ_d and is taken as the yield in the following momentum-dependent intervals: $-5 < \chi_d < -4$ for the first two momentum bins, $-4 < \chi_d < -3$ for the next two momentum bins, and $-3 < \chi_d < -2$ for the last bin. The efficiencies are all about 97%, except for the lowest momentum bin, where it is about 88% due to the lowside resolution tail. Our systematic error on the dE/dx efficiency comes from propagating the error on N_d quoted above.

The width of χ_d varies with momentum even after our recalibration, especially in the lowest momentum bin. We
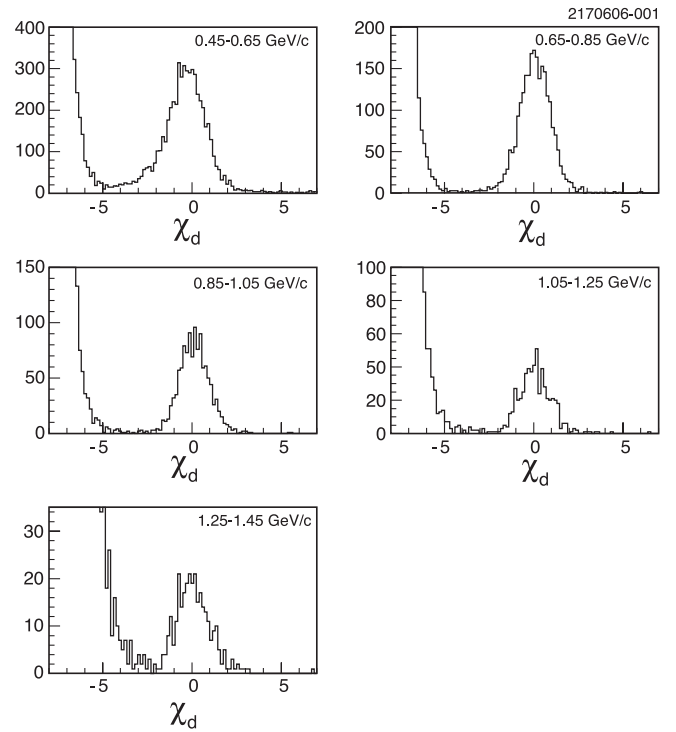

FIG. 2. Deuteron χ_d distributions (dE/dx normalized deviation) in different deuteron momentum bins.

determine our sensitivity by reweighting the momentum distribution in this bin to better reflect the data, and include an additional systematic error on the efficiency.

C. Systematic uncertainty summary

We now summarize our systematic uncertainties; in each case, we give the range across the five momentum bins. The total efficiency uncertainty, including track finding, selection criteria, and yield extraction from the χ_d plot, ranges from 4.5% to 16%. In addition to systematic issues discussed earlier in this section, we also considered the agreement between data and MC simulations of the number of photons associated with tracks in the RICH detector and the stability of results for variations in track-selection criteria. The number of Υ(1S) [Υ(2S)] in our data sample has an uncertainty of 1.4% [1.5%] and the continuum luminosity is known to 2%. The resulting total systematic uncertainties range from 6.1% to 16.0%. These are on average comparable to the statistical uncertainties in the case of the Υ(1S) result, and smaller than statistical errors in all other cases.

V. RESULTS

A. Antideuteron production in Υ(1S)

Table I shows the observed number of events from Υ(1S) resonance data, off-resonance data, and Δr and Δz sidebands in the on-resonance data. After subtracting the

TABLE II. Efficiency-corrected antideuteron yields and differential branching rations for Υ(1S) data in momentum bins.

| Momentum (GeV/c)	Corrected yield	Corrected direct yield	$d\mathcal{B}^{dir}/dp$ (10^{-5} (GeV/$c)^{-1}$)
0.45–0.65	85.6 ± 14.3	82.1 ± 16.4	2.2 ± 0.5 ± 0.2
0.65–0.85	111.3 ± 14.2	109.7 ± 15.0	3.0 ± 0.4 ± 0.2
0.85–1.05	106.2 ± 13.8	106.2 ± 14.5	2.9 ± 0.4 ± 0.3
1.05–1.25	92.5 ± 12.6	92.5 ± 13.8	2.5 ± 0.4 ± 0.2
1.25–1.45	60.2 ± 12.7	55.5 ± 14.1	1.5 ± 0.4 ± 0.2

FIG. 3. Momentum dependence of antideuteron production in Υ(1S) decays observed by CLEO (filled circles) and ARGUS (open diamonds). The solid line shows the fit described in the text; the dashed portion is an extrapolation beyond the momentum range which we observe.

latter sidebands and properly scaled continuum contributions, and correcting for efficiency, we get the number of $\bar{d}$ events produced by Υ(1S) decays shown in Table II. The direct yield column includes a larger continuum scale factor which accounts for the contribution in which $b\bar{b}$ reannihilate to a virtual photon and form a $q\bar{q}$ pair whose fragmentation products contain an antideuteron. We use this column to get the yield from so-called *direct* decays mediated by ggg and $gg\gamma$ hadronization.

To get the antideuteron yield in the full momentum range, we fit to the Maxwell distribution as used in fireball models [16],

$$f(p) \equiv a\beta^2 \exp(-E/b), \qquad (4)$$

where $\beta = pc/E$, and a and b are free parameters. We include as a systematic uncertainty the effect of variations of the shape parameter b within the statistical errors of the fit; we do not include any systematic uncertainty for the accuracy of the model itself. The resulting fit to the CLEO data is shown, along with the earlier ARGUS result, in Fig. 3. Much of the CLEO systematic error is correlated point-to-point, but statistics still dominate the uncertainty. Note that the ARGUS data extends to higher momentum due to their time-of-flight system for particle identification. We also note that ARGUS combined Υ(1S) and Υ(2S) yields to extract a more precise ggg rate; it is not clear what was assumed about possible χ_{bJ} production. However, it seems most likely that the difference in our results is largely statistical; ARGUS has 19 signal events from both resonances combined.

The final branching ratio per direct Υ(1S) → ggg, $gg\gamma$ decay is

$$\mathcal{B}^{dir}(\Upsilon(1S) \to \bar{d}X) = (3.36 \pm 0.23 \pm 0.25) \times 10^{-5}. \quad (5)$$

For this calculation, we have used only the number of Υ(1S) which decay via $ggg, gg\gamma$ as our normalization and subtracted a small amount of yield due to $b\bar{b}$ reannihilation to γ^* based on the observed off-resonance continuum yield. The more inclusive "conventional" branching ratio result is

$$\mathcal{B}(\Upsilon(1S) \to \bar{d}X) = (2.86 \pm 0.19 \pm 0.21) \times 10^{-5}. \quad (6)$$
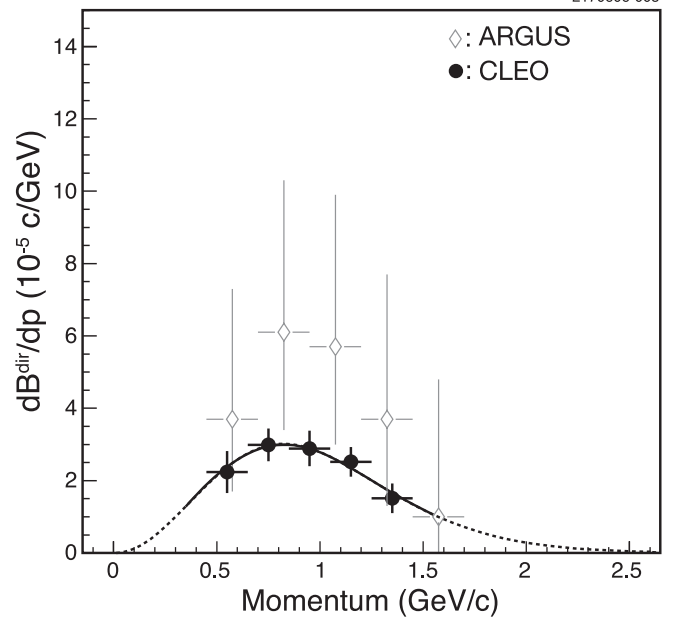
B. d production in Υ(1S)

Given that the deuteron signal is expected to be identical to the antideuteron signal, but with very much larger backgrounds, analyzing for deuterons would not contribute much statistically to this analysis. However, we can use deuteron production as a consistency check on our antideuteron measurement. We make this comparison for the restricted momentum range 0.6–1.1 GeV/c where the signal-to-noise is best.

Since none of the backgrounds described above peak in both Δr and Δz, we use a sideband subtraction to remove them. Empirically, we observe that Δr sidebands are very flat and we therefore subtract Δr sidebands from the good Δr sample and fit the resulting Δz distribution to a Gaussian peak plus a polynomial background. This procedure is displayed in Fig. 4. Here, we only use deuterons which satisfy $-2 < \chi_d < +3$ and ignore the small backgrounds from other particle types. The resulting deuteron yield is 352.8 ± 88.6, about 1.7 standard deviations from the antideuteron yield of 201.0 ± 14.2 in the same 0.6–1.1 GeV/c momentum range. The Δz width is somewhat narrower but similar to that for antideuterons.

C. Discussion of $\bar{d}$ baryon number compensation

Another way to explore consistency of the d and $\bar{d}$ yields is to employ baryon number conservation. Assuming many of the $\bar{d}$ (d) events are compensated by pp or pn ($\bar{p}\bar{p}$ or $\bar{p}\bar{n}$), requiring at least one p ($\bar{p}$) in the event may decrease
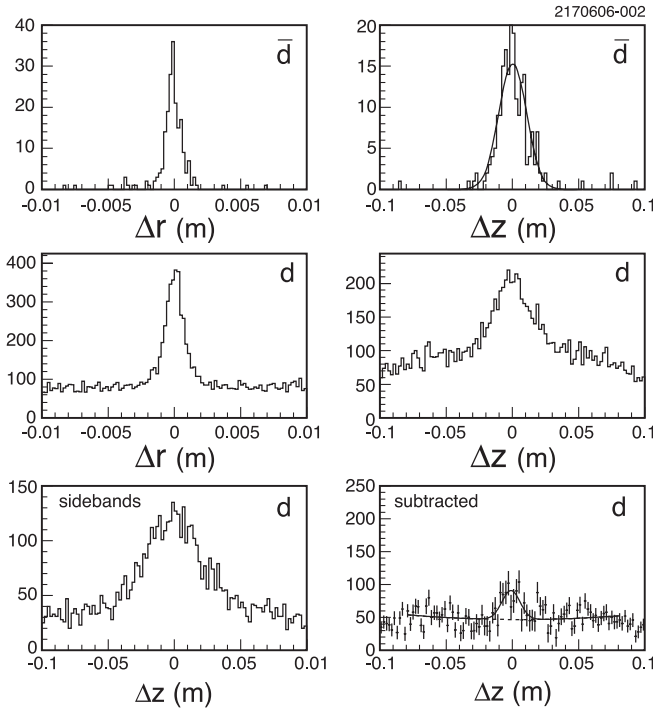
FIG. 4. Antideuteron and deuteron sample distributions for the momentum range 0.6–1.1 GeV/c in the $\Upsilon(1S)$ data. Top row: Δr and Δz for antideuterons. Middle row: Δr and Δz for deuterons. Bottom left: Δz for deuterons in Δr sidebands. Bottom right: Fit to Δz for deuterons after subtraction of the Δr sidebands in the previous panel. The signal Gaussian width is fixed to the antideuteron signal width from the fit to data in the upper right panel.

FIG. 5. d and $\bar{d}$ yields in the momentum range 0.45–1.45 GeV/c with additional criteria as described. Top row: χ_d for deuterons (left) and antideuterons (right) with all standard cuts, including $-2 < \chi_d < +3$. Second row: As above, but requiring at least one antiproton (left) or proton (right) candidate in addition. Third row: As above, but requiring two antiproton (left) or two proton (right) candidates instead. Fourth row: Δr and Δz for deuterons with $n_p > 0$. The curve on the left shows a fit to a signal Gaussian plus a polynomial background. Fifth row: Δr and Δz for deuterons with $n_p = 2$.

background appreciably. As shown in Fig. 5 and summarized in Table III, after the standard selection criteria, we begin with 13140 deuterons and 338 antideuterons candidates (signal plus background). Our proton identification requirements are: $|\chi_p| < 4$ for 0.30–0.85 GeV/c, and $|\chi_p| < 3$ for 0.85–1.15 GeV/c. Here, χ_p is a normalized dE/dx deviation with respect to the proton hypothesis and we do not accept candidates outside the two contiguous momentum windows indicated above. With this definition of protons, we can study the effect of cuts on the number, n_p, of protons (antiprotons) in antideuteron (deuteron) events. If we require $n_p > 0$, we are left with 149 $\bar{d}$ and 898 d; while the nondecay deuterons are very much reduced, the asymmetry indicates residual background from random antiprotons not associated with any baryon number compensation. This is further verified by examining the Δr, Δz distributions in the fourth row of Fig. 5. The excess is consistent with a spurious deuteron in coincidence with a real physics event containing the antiproton. A fit to the Δr distribution yields 122.8 ± 16.9 events for the sharp peak, which is now consistent with the antideuteron yield. Adding a requirement of $n_p \geq 2$, we obtain 31 $\bar{d}$ and 35 d, which are quite consistent with equality, implying that most spurious d have been removed. (Note that we never
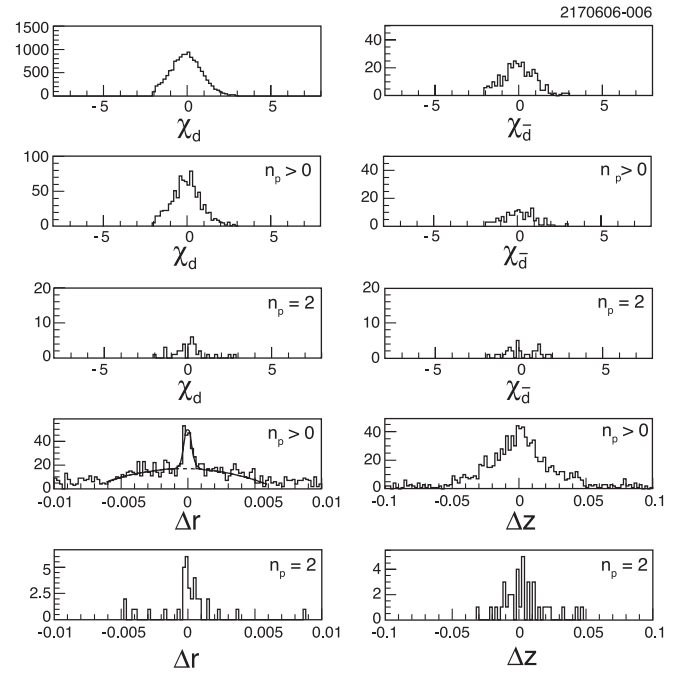
observed $n_p > 2$.) The remaining d events peak well both in Δr and Δz, as expected.

Returning to just the clean antideuteron sample, we can take a more quantitative look at baryon number conservation. By considering the effect of proton-finding efficiency, we can determine approximately how baryon compensation is distributed among pp, pn, np, nn; we will consider compensation by a d later.

In the $-2 < \chi_d < +3$ antideuteron signal region, we observe 338 candidate events from the $\Upsilon(1S)$ data sample. Each of these events contains only 1 antideuteron. Among these 338 events: 189 events contain no protons, 118 events contain 1 proton, and 31 events contain 2 protons.

TABLE III. Antideuteron and deuteron yields from $\Upsilon(1S)$ data with requirements on accompanying protons and antiprotons.

Standard cuts, plus:	Number of antideuteron candidates	Number of deuteron candidates
$\cdots$	338	13 140
$>0p/>0\bar{p}$	149	898
$\geq 2p/\geq 2\bar{p}$	31	35

TABLE IV. Antideuteron yields from $\Upsilon(1S)$ decay for various numbers of accompanying protons.

	All	$n_p = 0$	$n_p = 1$	$n_p = 2$
Observed	338	189	118	31
Predicted	⋯	166	142	30

Assuming $\bar{d}$ is compensated by pp, pn, np, nn (neglecting d for now) with an equal probability of 25%, we may estimate what is expected, given a proton-finding efficiency. We cannot distinguish pn and np, but it makes the assumed equality clearer to list them separately. For the proton identification cuts given above, the efficiency is about 60%, where we assume the spectrum of protons accompanying deuterons is similar to the inclusive proton spectrum. Part of the loss of efficiency is due to protons with momenta outside our accepted range of 0.30–1.15 GeV/c.

Folding in this approximate efficiency, we predict 30 events containing 2 protons, with 31 observed, and 142 events containing 1 proton, with 118 observed, as summarized in Table IV. Within the limits of our uncertainties and assumptions, our data is consistent with baryon number

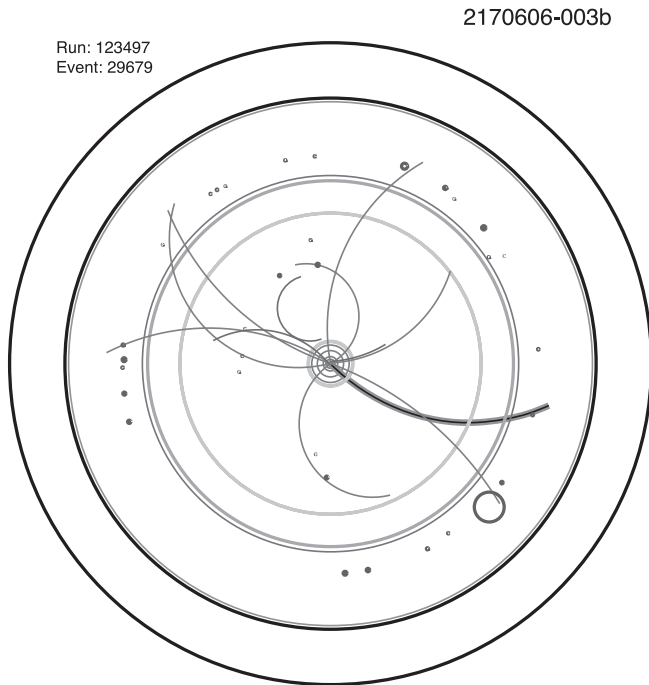FIG. 6. An $\Upsilon(1S) \rightarrow 3\pi^+3\pi^- d\bar{d}X$ candidate event in the CLEO detector, viewed along the beam axis. The d track ($p = 0.55$ GeV/c) is highlighted. The $\bar{d}$ track ($p = 0.84$ GeV/c) is the one with most energetic calorimeter shower; the circle size is proportional to the shower energy. The difference between the center-of-mass energy and the total energy of observed particles, based on tracking and particle identification, is about 120 MeV.

conservation occurring with roughly equal probabilities for accompanying pp, pn, np, or nn.

It is also interesting to look for compensation of an antideuteron by a deuteron; this is found to occur at the 1% level. Figure 6 shows one of our four possible $d\bar{d}X$ events, which is nearly fully reconstructed. Inspection of these four $d\bar{d}$ candidate events reveals that one of them is consistent with a through-going deuteron track (presumably from a cosmic-ray interaction) faking a $d\bar{d}$ pair. The remaining three are consistent with true $d\bar{d}$. Through-going deuterons might constitute a non-negligible background to our antideuteron yield, if the inward deuteron track passed our antideuteron cuts, but the outgoing deuteron fails. Therefore, we have searched for such events with relaxed cuts. We find none in the Δr and Δz sidebands, nor do we find any antideuteron candidate events where there is a lower-quality track candidate failing our cuts back-to-back with our candidate track. We conclude that this faking mechanism is rare and the one event seen was a somewhat unlikely occurrence for our data sample size.

D. $\bar{d}$ production in 2S, 4S, and continuum

We now summarize results from other Υ resonances and the continuum.

In $\Upsilon(2S)$ data, 69 antideuteron events are observed. This sample has the same background sources as the $\Upsilon(1S)$ data, but contains several possible sources of antideuteron signal. These include: (i) $\Upsilon(2S) \rightarrow \Upsilon(1S)X$, followed by $\Upsilon(1S) \rightarrow \bar{d}X'$, (ii) $\Upsilon(2S) \rightarrow ggg$, $gg\gamma$, and (iii) $\Upsilon(2S) \rightarrow \gamma\chi_{bJ}X$, followed by $\chi_{bJ} \rightarrow \bar{d}X'$. We may subtract process (i) based on known branching ratios. Separating (ii) and (iii), for example, by looking for the transition γ in (iii), is not feasible with our limited statistics. However, we can *assume* that the rate for the direct decay (ii) is equal to the analogous $\Upsilon(1S)$ process, and look for any excess from χ_{cJ} decays. This is interesting since the χ_{cJ} decay via gg for $J = 0$, 2 and via $gq\bar{q}$ for $J = 1$ and thus access distinct hadronization processes.

After background subtractions analogous to the $\Upsilon(1S)$ case, we find 58.3 ± 8.6 signal events, which translates to

$$\mathcal{B}(\Upsilon(2S) \rightarrow \bar{d} + X) = (3.37 \pm 0.50 \pm 0.25) \times 10^{-5}.$$
$$(7)$$

To isolate this rate, we subtract contributions from the processes $e^+e^- \rightarrow \Upsilon(2S) \rightarrow \pi\pi\Upsilon(1S)$ and $e^+e^- \rightarrow \Upsilon(2S) \rightarrow \gamma\gamma\Upsilon(1S)$ (two-photon transitions via the χ_{bJ} states) assuming that these processes dominate inclusive $\Upsilon(1S)$ production. We must further assume that direct ggg, $gg\gamma$ decays of the $\Upsilon(2S)$ produce antideuterons at the same rate as the $\Upsilon(1S)$. We are left with an insignificant excess, and extract a 90% C.L. upper limit for a weighted average of the χ_{bJ} states of

$$\sum_J (\mathcal{B}(\Upsilon(2S) \to \gamma\chi_{bJ}(1P))$$

$$\times \mathcal{B}(\gamma\chi_{bJ}(1P) \to \bar{d}X)) \Big/ \sum_J \mathcal{B}(\Upsilon(2S) \to \gamma\chi_{bJ}(1P))$$

$$< 1.1 \times 10^{-4}. \tag{8}$$

This limit is not stringent enough to draw firm conclusions on antideuteron production in these distinct gg and $gq\bar{q}$ hadronization processes in contrast to ggg, $gg\gamma$.

In $\Upsilon(4S)$ data, 3 $\bar{d}$ candidates are observed. Based on Δr and Δz sidebands and the continuum data, we expect 5.2 background events. For both this limit and the following continuum production limit, we ignore any possible backgrounds in the χ_d distribution. We obtain a 90% C.L. upper limit, using the Feldman-Cousins method [17], of

$$\mathcal{B}(\Upsilon(4S) \to \bar{d}X) < 1.3 \times 10^{-5}. \tag{9}$$

This limit is not very stringent in view of the dominance of $B\bar{B}$ decays of the $\Upsilon(4S)$.

A 90% C.L. upper limit result for continuum production is also obtained, based on 6 events with 1.5 expected background:

$$\sigma(e^+e^- \to \bar{d}X) < 0.031 \text{ pb}, \qquad \text{at } \sqrt{s} = 10.5 \text{ GeV}. \tag{10}$$

Given that the continuum hadronic cross section at $\sqrt{s} = 10.5$ GeV exceeds 3000 pb, we see that fewer than 1 in 10^5 $q\bar{q}$ hadronizations results in antideuteron production, noticeably less than for ggg, $gg\gamma$ hadronization.

VI. CONCLUSIONS

Using CLEO data, we have studied antideuteron production from $\Upsilon(nS)$ resonance decays and the nearby continuum. $\Upsilon(1S)$ and $\Upsilon(2S)$ production rates are presented separately for the first time and combined to limit antideuteron production from $\chi_{bJ}(1P)$ states. First limits on production from the $\Upsilon(4S)$ and an improved continuum production limit are given.

The results confirm a small but significant rate from hadronization of $\Upsilon(nS) \to ggg$, $gg\gamma$ decays, for $n = 1, 2$. However, no significant production from $q\bar{q}$ hadronization is observed; our $q\bar{q}$ limit is more than 3 times smaller than the observed rate from ggg hadronization. Thus, the results indicate that antideuteron production is enhanced in ggg, $gg\gamma$ hadronization relative to $q\bar{q}$.

We observe that baryon number conservation is accomplished with approximately equal amounts of accompanying pp, pn, np, nn. We also found three $d\bar{d}$ events; it is not immediately clear if double coalescence from initial baryons and antibaryons can accommodate this rate, or if this is evidence for a more primary sort of (anti)deuteron production in the hadronization process.

[1] H. Albrecht *et al.* (ARGUS Collaboration), Phys. Lett. B **236**, 102 (1990).

[2] S. Schael *et al.* (ALEPH Collaboration), Phys. Lett. B **639**, 192 (2006). A detailed list of earlier experiments is provided by these authors.

[3] D. E. Dorfan *et al.*, Phys. Rev. Lett. **14**, 1003 (1965); T. Alexopoulos *et al.* (E735 Collaboration), Phys. Rev. D **62**, 072004 (2000); A. Aktas *et al.* (H1 Collaboration), Eur. Phys. J. C **36**, 413 (2004).

[4] H. H. Gutbrod *et al.*, Phys. Rev. Lett. **37**, 667 (1976); H. Sato and K. Yazaki, Phys. Lett. **98B**, 153 (1981).

[5] R. Akers *et al.* (OPAL Collaboration), Z. Phys. C **67**, 203 (1995).

[6] G. Gustafson and J. Hakkinen, Z. Phys. C **61**, 683 (1994).

[7] S. Behrends *et al.* (CLEO Collaboration), Phys. Rev. D **31**, 2161 (1985); R. A. Briere *et al.* (CLEO Collaboration), hep-ex/0607052.

[8] J. L. Rosner, Phys. Rev. D **69**, 094014 (2004).

[9] M. Karliner *et al.*, J. High Energy Phys. 12 (2004) 045.

[10] T. S. Hill, Nucl. Instrum. Methods Phys. Res., Sect. A **418**, 32 (1998).

[11] D. Peterson *et al.*, Nucl. Instrum. Methods Phys. Res., Sect. A **478**, 142 (2002).

[12] M. Artuso *et al.*, Nucl. Instrum. Methods Phys. Res., Sect. A **502**, 91 (2003); **554**, 147 (2005).

[13] Y. Kubota *et al.*, Nucl. Instrum. Methods Phys. Res., Sect. A **320**, 66 (1992).

[14] R. Ammar *et al.* (CLEO Collaboration), Phys. Rev. D **57**, 1350 (1998).

[15] G. S. Adams *et al.* (CLEO Collaboration), Phys. Rev. Lett. **94**, 012001 (2005).

[16] R. Hagedorn, Nuovo Cimento Suppl. **3**, 147 (1965); Nucl. Phys. **B24**, 93 (1970).

[17] G. J. Feldman and R. D. Cousins, Phys. Rev. D **57**, 3873 (1998).